Supplementary Information

for

Mms22-Rtt107 axis attenuates the DNA damage checkpoint and the stability of the Rad9 checkpoint mediator

Bingbing Wan, Danying Guan, Shibai Li, Tzippora Chwat-Edelstein, Xiaolan Zhao

Supplementary Fig.1 to 6

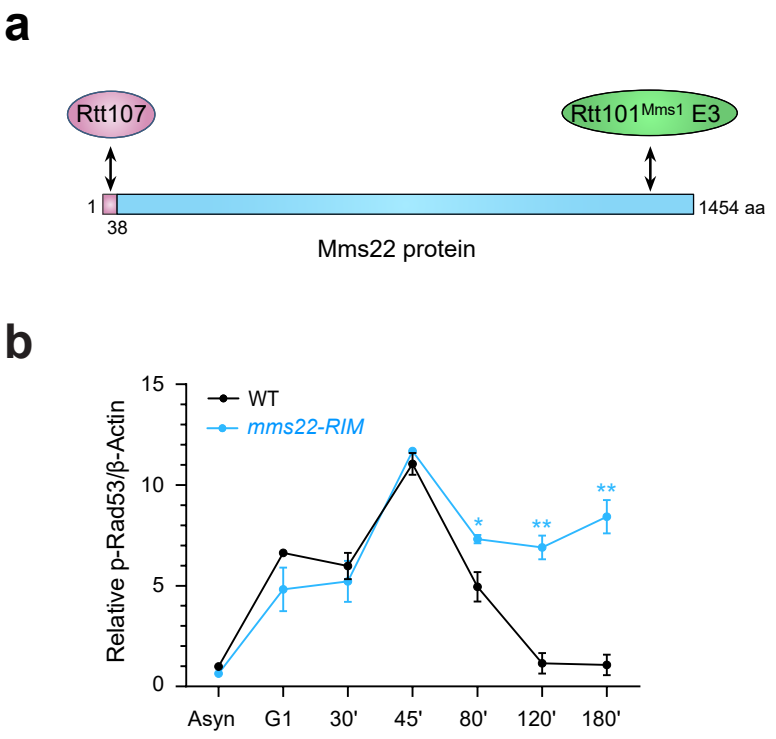

Supplementary Fig. 1. | *mms22*^{RIM} is a separation-of-functional allele that disrupts Mms22-Rtt107 binding and causes increased levels of Rad53 phosphorylation.

a Schematic showing that the N-terminal region of Mms22 binds to Rtt107, and its C-terminal region interacts with the Mms1 subunit of the Rtt101^{Mms1} ubiquitin E3.

b Quantification of the active form of Rad53 in the time course done as in Figs. 1c and 1d. Averages and Standard Deviation (SDs) based on two biological duplicates are shown; Statistical analysis was performed by one-tailed unpaired Student's *t*-test. * $p < 0.05$, ** $p < 0.01$.

Source data are provided as a Source Data file.

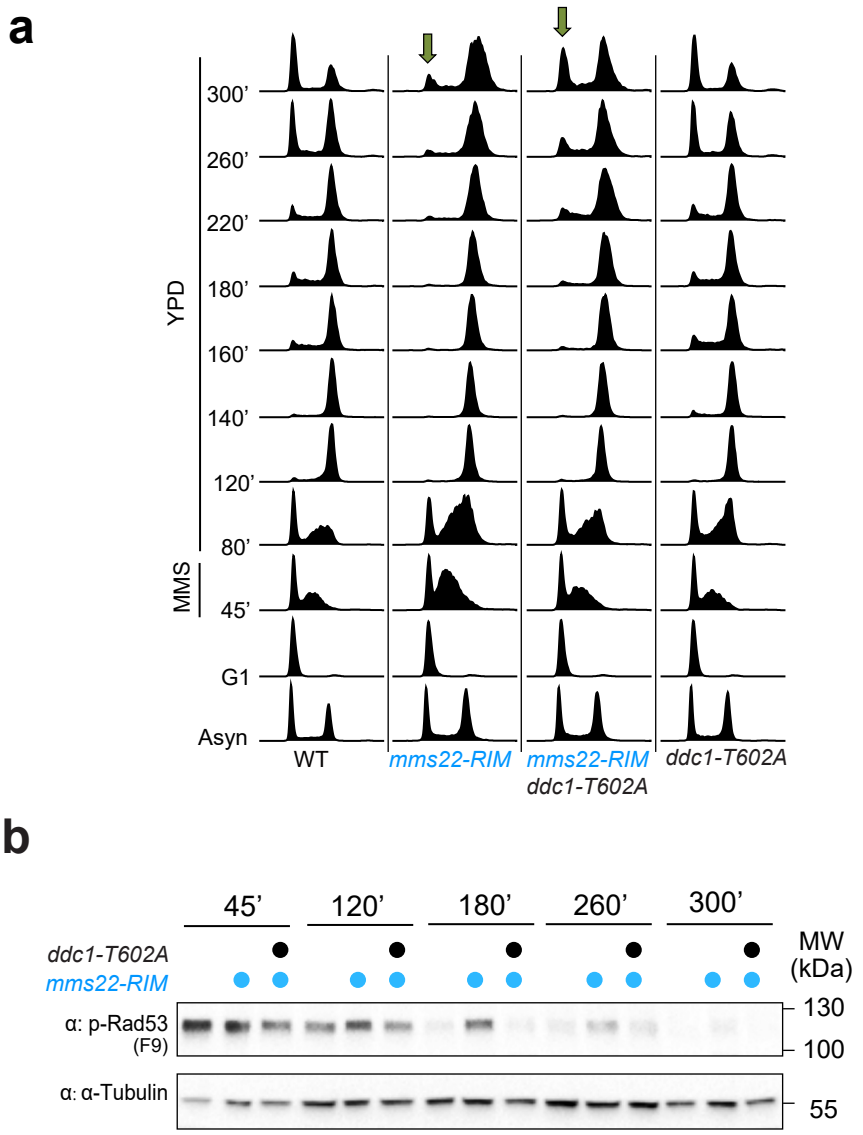

Supplementary Fig. 2. | Persistent checkpoint seen in *mms22^{RIM}* cells are rescued by a mild *ddc1* mutant allele.
a *mms22^{RIM}* defect in exiting G2/M phase is improved by *ddc1-T602A*. Experiments were done, and data are presented as in Fig. 2c. The experiments were conducted using two independent biological samples per genotype with similar results obtained.
b Persistence of Rad53 phosphorylation in *mms22^{RIM}* cells is suppressed by *ddc1-T602A*. Experiments were done, and data are presented as in Fig. 2e. The experiments were conducted using two independent biological samples per genotype with similar results obtained.
Source data are provided as a Source Data file.

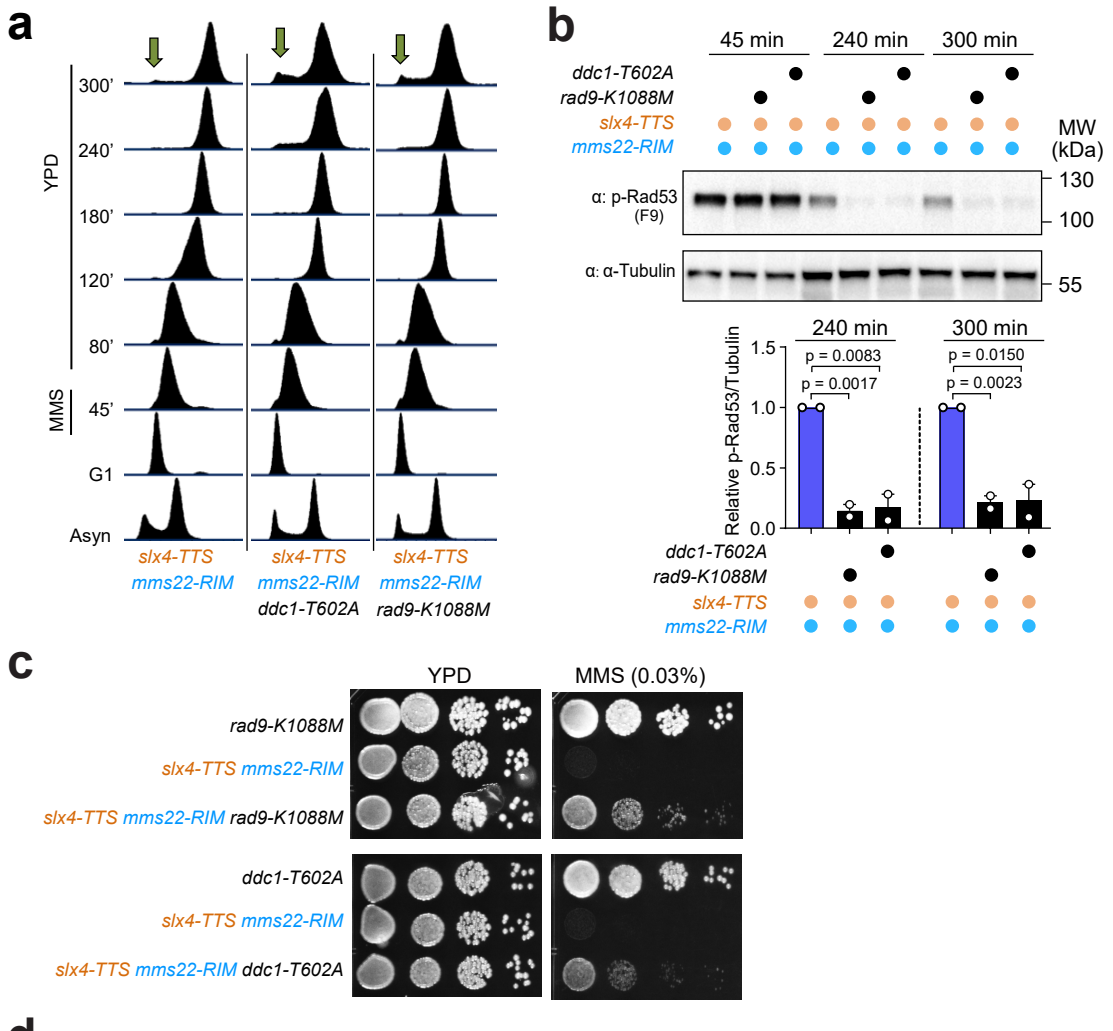

Supplementary Fig. 3. | Phenotypical rescue of the *mms22^{RIM}slx4^{TTS}* double mutant by the *rad9* and *ddc1* checkpoint defect alleles.

a Defects in exiting G2/M phase by the *mms22^{RIM}slx4^{TTS}* double mutant cells are improved by *ddc1-T602A* or *rad9-K1088M*. Experiments were conducted, and data are presented as in Fig. 2c.

b Persistence of Rad53 phosphorylation in *mms22^{RIM}slx4^{TTS}* double mutant cells is suppressed by *ddc1-T602A* or *rad9-K1088M*. Experiments were conducted, and data are presented as in Fig. 3b.

c The MMS sensitivity of *mms22^{RIM} slx4^{TTS}* cells is suppressed by *ddc1-T602A* or *rad9-K1088M*. Experiments were conducted as in Fig. 1b.

d *rtt107Δ* cells exhibit stronger sensitivities to genotoxins than the *mms22^{RIM} slx4^{TTS}* double mutant cells. Experiments were conducted as in Fig. 1b. Dashed lines indicate the removal of rows of cells unrelated to this work.

Source data are provided as a Source Data file.

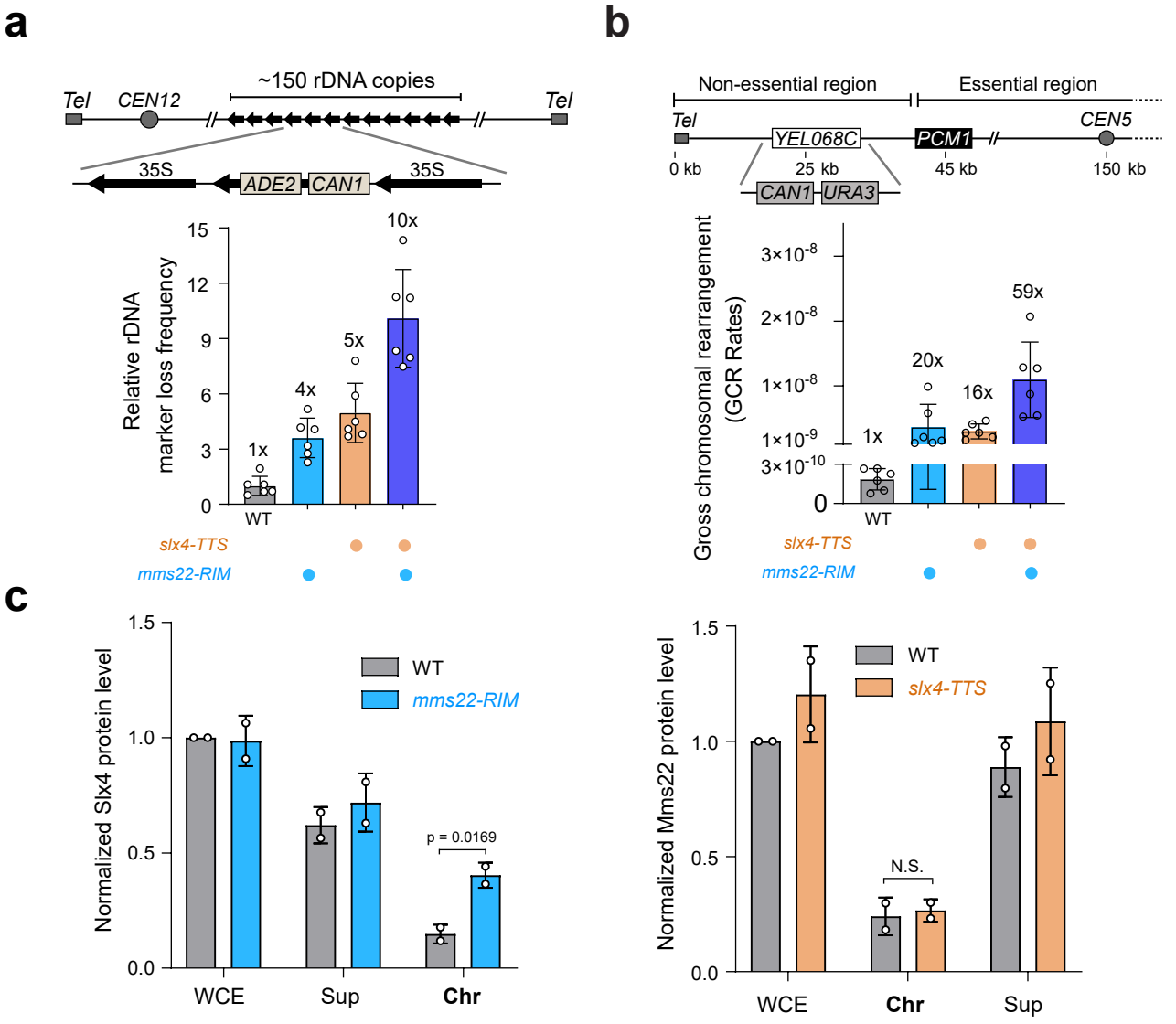

Supplementary Fig. 4. | Mms22 and Slx4 mutants act in parallel pathways.
a rDNA marker loss results. Top: schematic of rDNA marker loss assay as described previously[53]. Bottom: averages of marker loss rates and SDs were calculated from at least six cultures and two biological duplicates.
b GCR assay results. Top: schematic of the GCR assay as described previously[52]. Bottom: median GCR rate for each genotype was calculated from at least six cultures and two biological duplicates. Error bars are the 95% confidence intervals.
c Quantification of Slx4 (left) and Mms22 (right) levels in wild-type verse mutant strains. Data were derived based on two biological replicates, and the result of one of these is shown in Fig. 3d. Averages and SEMs are indicated; statistical analysis was performed by one-tailed unpaired Student's *t*-test. N. S.: not statistically significant. Source data are provided as a Source Data file.

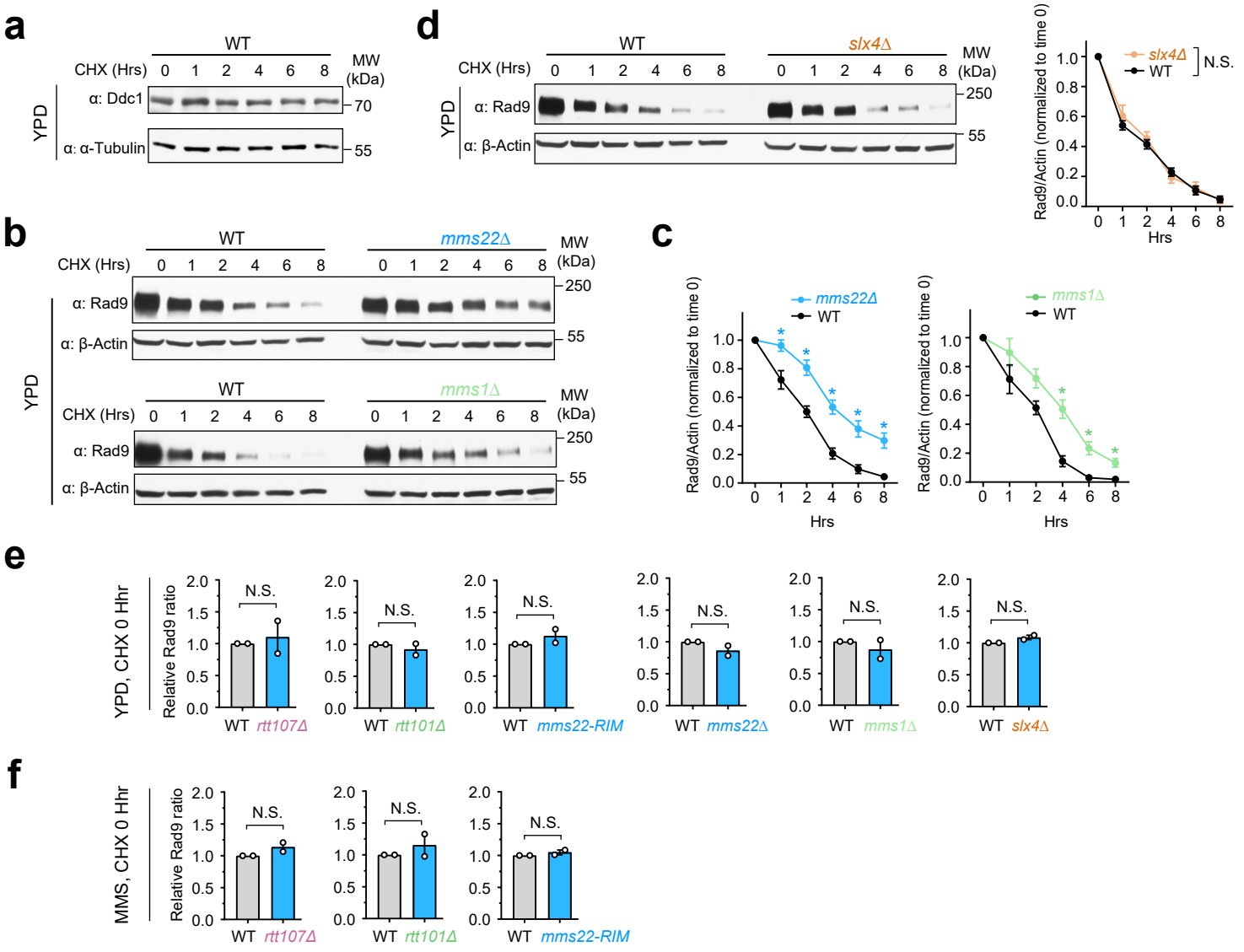

Supplementary Fig. 5. | Examination of Rad9 and Ddc1 protein stability.
a Ddc1 protein levels are largely unchanged during an eight-hour time course in the presence of CHX. Experiments were conducted, and data are presented as in Fig. 4a using two strains per genotype that gave similar results.
b Rad9 protein stability is increased in cells lacking Mms22 and Mms1. Experiments were conducted and data are presented as in Fig. 4a. Experiments were conducted using two strains per genotype with similar results obtained.
c Rad9 protein stability quantification. Quantification of Rad9 protein levels in reference to the loading control of actin levels from at least two biological duplicates is plotted. Averages and SEMs are indicated; statistical analysis for each time point was performed by one-tailed unpaired Student's *t*-tests. * $p < 0.05$.
d Rad9 protein stability is not affected by *slx4*Δ. Left: a representative immunoblot showing that Rad9 levels during CHX treatment were similar between wild-type and *slx4*Δ cells. Right, Quantification of Rad9 protein levels during the time courses in reference to the loading control of actin levels from two biological duplicates. Averages and SEMs are indicated; statistical analysis was performed by two-tailed unpaired Student's *t*-test. N. S.: not significant.
e-f Rad9 protein levels in wild-type and mutant cells are compared before CHX treatment either in YPD media (e) or in media containing MMS (f). Rad9 protein levels from two strains per genotype were quantified based on immunoblots as exemplified in Fig. 4a and normalized to β-Actin signals. Averages and SEMs are indicated; statistical analysis was performed by two-tailed unpaired Student's *t*-test. N. S.: not significant.
Source data are provided as a Source Data file.

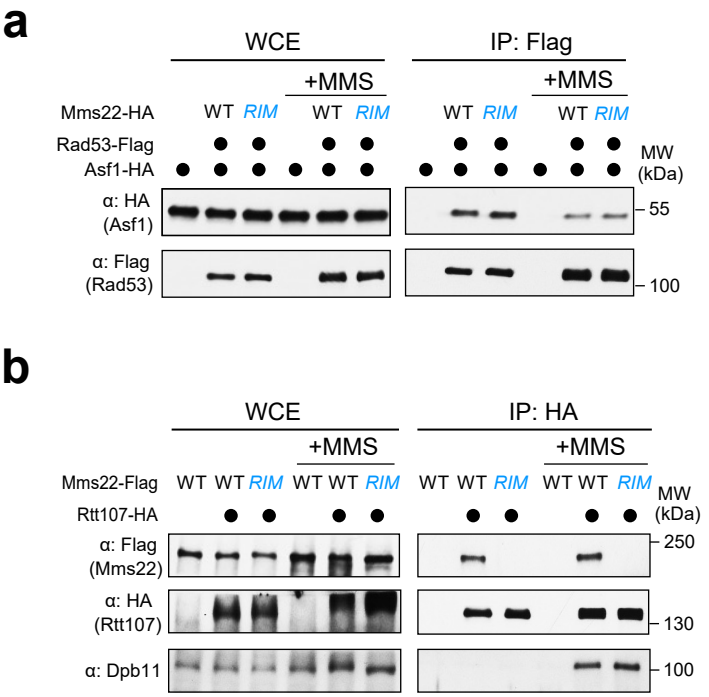

Supplementary Fig. 6. | *mms22^{RIM}* does not alter the Rad53-Asf1 or the Rtt107-Dpb11 association.

a *mms22^{RIM}* does not affect Rad53-Asf1 interaction based on co-immunoprecipitation results. WCE was input control of the immunoprecipitation.

b *mms22^{RIM}* disrupts Mms22 interaction with Rtt107 but does not affect the Rtt107-Dpb11 association based on co-immunoprecipitation results.

The experiments were conducted using two strains per genotype with similar results obtained.

Source data are provided as a Source Data file.